RSC Advances

ROYAL SOCIETY OF CHEMISTRY

PAPER

View Article Online
View Journal | View Issue

Cite this: *RSC Adv.*, 2026, **16**, 14492

Green synthesis and antibacterial activity of zinc oxide nanoparticles using *Croton macrostachyus* Hochst. ex Delile extracts

Tesfaye Haile Habtemariam, *[a] Senait Haille Anjullo[a] and Gedif Meseret Abebe[b]

The green synthesis of zinc oxide nanoparticles (ZnO-NPs) using plant extracts is an eco-friendly and economical process compared with existing methods. The present investigation utilized the leaf and seed extracts of *Croton macrostachyus* Hochst. ex Delile to biosynthesize ZnO-NPs using a green technique with zinc acetate as the precursor at 80 °C for 60 minutes. XRD analysis proved the hexagonal structure of the Wurtzite ZnO-NPs, with average crystallite dimensions of approximately 40 nm. The estimated band gaps using UV-Visible spectroscopy were in the range of 3.17–3.19 eV, and FTIR, SEM, XPS, and EDS studies proved the functional groups and element contents of ZnO-NPs, in which trace levels of Ca and Mg were present in the extracts. The ZnO-NPs derived from the green synthesis method displayed high antibacterial efficacy against Gram-positive *Staphylococcus aureus* and Gram-negative *Pseudomonas aeruginosa* and *Klebsiella pneumoniae*, which surpassed the antibacterial efficacy of the crude extracts. The green synthesis of ZnO NPs using *Croton macrostachyus* extracts thus presents promising results in relation to their possible antibacterial applications in the biomedical field and green nanotechnology.

Received 27th January 2026
Accepted 6th March 2026

DOI: 10.1039/d6ra00724d

rsc.li/rsc-advances

1 Introduction

Nanoscience and nanotechnology have made vast progress over the last few years, and this has led to innovations within many sectors such as electronics, cosmetics, pharmaceuticals, and textile industries using nanoparticles (NPs) with sizes ranging from 1 nm to 100 nm.[1,2] Among the various types of nanomaterials, metal and metal oxide nanoparticles including aluminum, nickel, silver, copper, iron, cerium dioxide, titanium dioxide, and zinc oxide are particularly prominent due to their unique properties and wide-ranging industrial applications.[3–6]

Metal oxide nanoparticles (MO NPs) are considered especially promising due to their distinctive physical, chemical, and biological properties, including high solubility, chemical stability, and adhesiveness.[7] Green synthesis of metal nanoparticles typically utilizes plant extracts as both reducing and stabilizing agents, with the addition of metal salt solutions often resulting in a visible color change that signifies nanoparticle formation.[8] Green synthesis takes advantage of the available phytochemicals in plant extracts, including flavonoids, proteins, polysaccharides, and alkaloids.[9]

Green chemistry is a sustainable approach in process development that adopts non-toxic and environmentally friendly processes. Green synthesis is a strategy that aims to synthesize nanoparticles using environmentally friendly processes and approaches that utilize green solvents and natural agents that require low energy.[10,11] Utilizing plant extracts in these methods offers several advantages: they act as both reducing and stabilizing agents, enable rapid synthesis under mild conditions (pressure, temperature, incubation time, and pH), and eliminate the need for additional capping agents, thereby minimizing the environmental impact of nanoparticle production.[12]

For the purpose of producing stable nanoparticles on a large scale, plants are the primary source.[13] Recent research reported the synthesis of zinc oxide nanoparticles (ZnO-NPs) using different plant extracts such as *Tabernaemontana divaricata* green leaf extract,[14] *Guava* leaf extract,[15] *Laurus nobilis* L. leaves aqueous extract,[16] and *Aloe barbadensis* miller leaf extract.[17] For the synthesis of ZnO NPs in this work, *Croton macrostachyus* Hochst. ex Delile (Bisana) leaf and seed extract serves as a bioreducing agent. The terms rush foil (English), Bakkaniisa (Afan Oromo), Bisana (Amharic), and Anika (Wolayita) are frequently used to refer to *Macrostachyus*. Traditionally, *C. macrostachyus* is used for the treatment of malaria, rabies, gonorrhea, wounds, diarrhea, hepatitis, jaundice, scabies, toothache, abdominal pain, cancer, typhoid, pneumonia, and gastrointestinal disorders, and as ethnoveterinary medicine.[18,19] The pharmacologic researches conducted on *C. macrostachyus* show that it possesses many pharmacologic actions such as anthelmintic, antibacterial, antimycobacterial, antidiarrheal,

---

[a] *Department of Chemistry, Wolaita Sodo University, Sodo, Ethiopia. E-mail: tesfaye.haile@wsu.edu.et*

[b] *Department of Biology, Wolaita Sodo University, Sodo, Ethiopia*

antifungal, anticonvulsant & sedative, antidiabetic, anti-inflammatory, antileish.[19]

Plants serve as 'green nanofactories' for the synthesis of nanoparticles, and there is growing interest among scientists in utilizing plant-mediated approaches for the green synthesis of ZnO NPs and their applications. The use of plant extracts offers several advantages: they are readily available, safe, non-toxic, and rich in natural reducing agents that facilitate the reduction of metal ions.[20] This helps lower time consumption, expenditure, and wastage in efforts to develop sustainable and environmentally-friendly technologies in the production chain. Green nanotechnology, also known as the photobiological approach, uses different plant materials like fruit, pulp, bark, root, leaves, and stems of plants in extracting phytochemicals needed in the nanotechnology production process.[10,20] These phytochemicals, including alcohols, proteins, flavonoids, and phenols, act as both reducing and stabilizing agents, with their negatively charged functional groups playing a key role in metal ion reduction and nanoparticle stabilization.[21–23]

Zinc oxide (ZnO) nanoparticles are among the most widely utilized metal oxide nanomaterials, owing to their diverse biological properties including antimicrobial, antioxidant, antidiabetic, anticancer, and anti-inflammatory activities as well as their applications in drug delivery, solar cells, photocatalysis, and personal care products.[24] Despite these benefits, there is a need for conducive methods that are environmentally friendly and efficient in synthesizing the nanoparticles. This research will specifically highlight the green synthesis of ZnO nanoparticles using the extract of the leaf and seeds of the *Croton macrostachyus* Hochst. ex Delile species. Although plant-mediated synthesis of ZnO nanoparticles has been extensively studied, this paper presents the first report on the use of both leaf and seed extracts of *Croton macrostachyus* Hochst. ex Delile for the bioreduction and stabilization of ZnO nanoparticles. This is due to the unique phytochemical composition of the plant that facilitated the synthesis of ZnO NPs with trace amounts of Ca and Mg. This is unusual in plant-mediated synthesis of metal oxide nanoparticles. The optimized conditions for the synthesis of ZnO NPs with trace amounts of Ca and Mg, with the use of *Croton macrostachyus* Hochst. ex Delile, produced a crystallite size of 40 nm with potent antibacterial activity. This paper has clearly demonstrated the use of a novel biological system that has a significant influence on the chemistry and morphology of ZnO nanoparticles. This is different from existing studies on plant-mediated synthesis of ZnO nanoparticles.

2 Materials and methods

2.1 Materials

The procedure of synthesizing biogenic zinc oxide (ZnO) nanoparticles (NPs) using the plant extracts for antibacterial purposes required different materials and agents. Zinc acetate dihydrate ($Zn(CH_3COO)_2 \cdot 2H_2O$) was used as the starting material for zinc ions, and deionized water ($d.H_2O$) and distilled water were used to prepare all solutions. Additionally, ferric chloride ($FeCl_3$), chloroform, anhydrous acetic acid, sulfuric acid (H_2SO_4), and Mayer's reagent were applied for the detection and screening of phytochemicals in the leaves and seeds of *Croton macrostachyus* Hochst. ex Delile. Gentamicin was used as positive controls in assessing antibacterial activity, while dimethyl sulfoxide (DMSO) was used as negative controls in testing inhibition zones for NPs and plant extracts. Nutrient agar, Mueller–Hinton agar, and nutrient broth were used as media for growing microorganisms, while saline solution was used for dilution and bioassay. The antimicrobial efficacy of the nanoparticles (NPs) and extracts was evaluated using the Gram-positive bacterium *Staphylococcus aureus* and the Gram-negative bacteria *Pseudomonas aeruginosa* and *Klebsiella pneumoniae*. Finally, plant extracts provided the biological molecules necessary for the biogenic synthesis of ZnO NPs.

2.2 Instrumentations

The samples were accurately weighed using the digital analytical balance (Model: PX84). The crystal structure of ZnO nanoparticles synthesized using the green technique was examined using the X-ray diffractometer (XRD, Model: XRD-7000 Shimadzu Co., South Korea), collecting XRD spectra within the 2θ angle of 10–80° using CuKα radiation at 40 kV and 30 mA. The crystallite sizes (D) of the powders were calculated using Scherrer's equation:

$$D = \frac{0.94\ \lambda}{\beta \cos \theta}$$

where λ is the X-ray wavelength, θ is Bragg's diffraction angle, and β is the peak width of the diffraction line at half of the maximum intensity. The optical properties of the biogenic ZnO NPs were evaluated using UV-Visible diffuse reflectance spectroscopy (UV-Vis-DRS, Model: JASCO V-78 UV-Vis) within the range of 200–800 nm. Fourier transform infrared (FTIR) spectroscopy (FT-IR, PerkinElmer Spectrum 65) was employed to identify the functional groups involved in the biosynthesized ZnO nanoparticles, with analysis conducted in the scanning range of 4000–400 cm^{-1} using samples ground and mixed with KBr pellets. Elemental composition was validated using X-ray Photoelectron Spectroscopy with a SPECS GmbH system equipped with a hemispherical energy analyzer PHOIBOS 150 9MCD and Energy-Dispersive X-ray Spectroscopy. The surface morphology of the biosynthesized ZnO nanoparticles was analyzed by Scanning Electron Microscopy (SEM, Model: JCM-6000Plus) by preparing thin films of the sample on a carbon-coated copper grid.

2.3 Plant collection

In February 2024, fresh leaf and seed of *Croton macrostachyus* Hochst. ex Delile were collected from Gununo, Damot Sore area of Wolaita, Ethiopia (Fig. 1). The leaves and seeds were well-rinsed using tap water and later distilled water to wash off any dust particles. Later, the leaves and seeds dried in the shade for a period of two weeks. The leaves and seeds, after drying, were ground into a fine powder using a pestle and a mortar. Finally, the leaves and seeds were packed in airtight containers at room temperature.

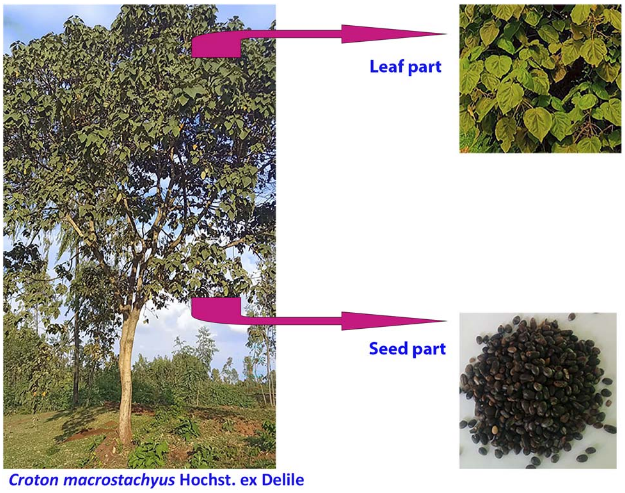

Fig. 1 *Croton macrostachyus* Hochst. ex Delile: this is a picture of a plant with a magnified leaf and a dried seed part.

2.4 Preparation of *Croton macrostachyus* Hochst. ex Delile leaf and seed extracts

A total of 10 g of dried, powdered *Croton macrostachyus* Hochst. ex Delile leaf and seed was separately mixed with 300 mL of deionized water (DI H_2O) in a 500 mL glass beaker. The mixture was heated in a water bath (HWS-24) at 60 °C for 1 hour. After heating, the extract was allowed to cool to room temperature. The aqueous solution was filtered using Whatman filter paper no. 1. The filtered solution of *Croton macrostachyus* Hochst. ex Delile leaf and seed extracts was refrigerated at 4 °C for storage.

2.5 Phytochemical analysis of leaf and seed extracts of *Croton macrostachyus* Hochst. ex Delile

2.5.1 Test for phenols and tannins. The leaf and seed extracts were each combined with 2 mL of a 2% $FeCl_3$ solution. Upon mixing, a blue-green color appeared, which is indicative of the presence of polyphenols and tannins. This is because of the interaction between the $FeCl_3$ and the phenolic compounds, which form a complex whose characteristic blue-green color can then be noted. The presence of these compounds is quite vital because polyphenols and tannins have been long recognized for their health benefits, which result from their antioxidant properties.[25]

2.5.2 Test for flavonoids. A qualitative assay was performed to assess the presence of flavonoids within leaf and seed extracts. The extract (2 mL) was mixed with distilled water (8 mL). The solution was filtered to remove particulate matter. Then, 4–5 drops of NaOH were added to the filtrate. A yellow-orange coloration was developed, which was regarded as positive for flavonoids.[26]

2.5.3 Test for saponins. A mixture of 2 mL of leaf and seed extract was combined with 8 mL of distilled water in a test tube. This mixture was then shaken vigorously for 30 seconds. The formation of a stable foam, which persisted even after 30 minutes, was taken as an indication of the presence of saponins. Saponins are known for their surfactant properties, which allow them to form stable foams. This characteristic is commonly used as a qualitative test for their presence in plant extracts.[27]

2.5.4 Test for steroids. In this experiment, we tried to determine if there were terpenoids present in the extracts of both the leaves and seeds by performing a common phytochemical test. To accomplish this, a mixture of 2 mL of extract from both the leaves and seeds was combined with 2 mL of chloroform. The mixture was allowed to evaporate to dryness. Subsequent to that, 2 mL of concentrated sulfuric acid (H_2SO_4) was added to the dried extract. The formation of a reddish-brown coloration at the interface indicated the presence of terpenoids. This color change is a positive result for the Salkowski test, which is commonly used to detect terpenoids in plant extracts.[28]

2.5.5 Test for alkaloids. To detect the presence of alkaloids, 2 mL of the leaf and seed extract was mixed with 2 mL of 1% HCl. The solution was then heated in a water bath for 10 minutes. After heating, 6–8 drops of Mayer's reagent were added. The appearance of orange precipitates revealed the presence of alkaloids. This technique corresponds to recent approaches that involved several steps in phytochemical screening.[29,30]

2.6 Synthesis of zinc oxide nanoparticles using *Croton macrostachyus* Hochst. ex Delile leaf and seed extracts

The synthesis of biogenic ZnO NPs is performed by a modification of the procedure detailed in the previous work[26] as shown in the Scheme 1. A 5 g sample of zinc acetate dihydrate (MW = 219.49 g mol^{-1}) was mixed with 50 mL of *Croton macrostachyus* Hochst. ex Delile leaf or seed extracts in a 150 mL beaker. The mixture was heated to 60 °C and 80 °C in a water bath (HWS-2T) for one hour until a white precipitate formed. The mixture was then allowed to settle overnight at room temperature. The liquid portion was decanted using a dropper, and the white precipitate was collected. The collected precipitate was left overnight in a hot air oven at 80 °C, resulting in the formation of a creamy paste. This paste was washed twice with a solution of deionized water and ethanol (3 : 1). After settling overnight, the liquid portion was removed using a dropper, and the washed creamy paste was dried in a hot air oven (GP-65B) at 80 °C for overnight. The dried paste was then transferred to a ceramic crucible cup and heated in furnance at 100 °C for 3 hours. The resulting white powder, identified as ZnO nanoparticles, was kept in an airtight container for further analysis.

2.7 Antimicrobial activities of synthesized zinc oxide nanoparticles

The antimicrobial activities of the synthesized zinc oxide nanoparticles (ZnO NPs) were assessed using a modified agar well diffusion method, as previously described.[31] This study focused on two Gram-negative bacteria (GNB), *Klebsiella pneumoniae* and *Pseudomonas aeruginosa*, and one Gram-positive bacterium (GPB), *Staphylococcus aureus*. The antibacterial activity of the biosynthesized ZnO NPs was tested and compared

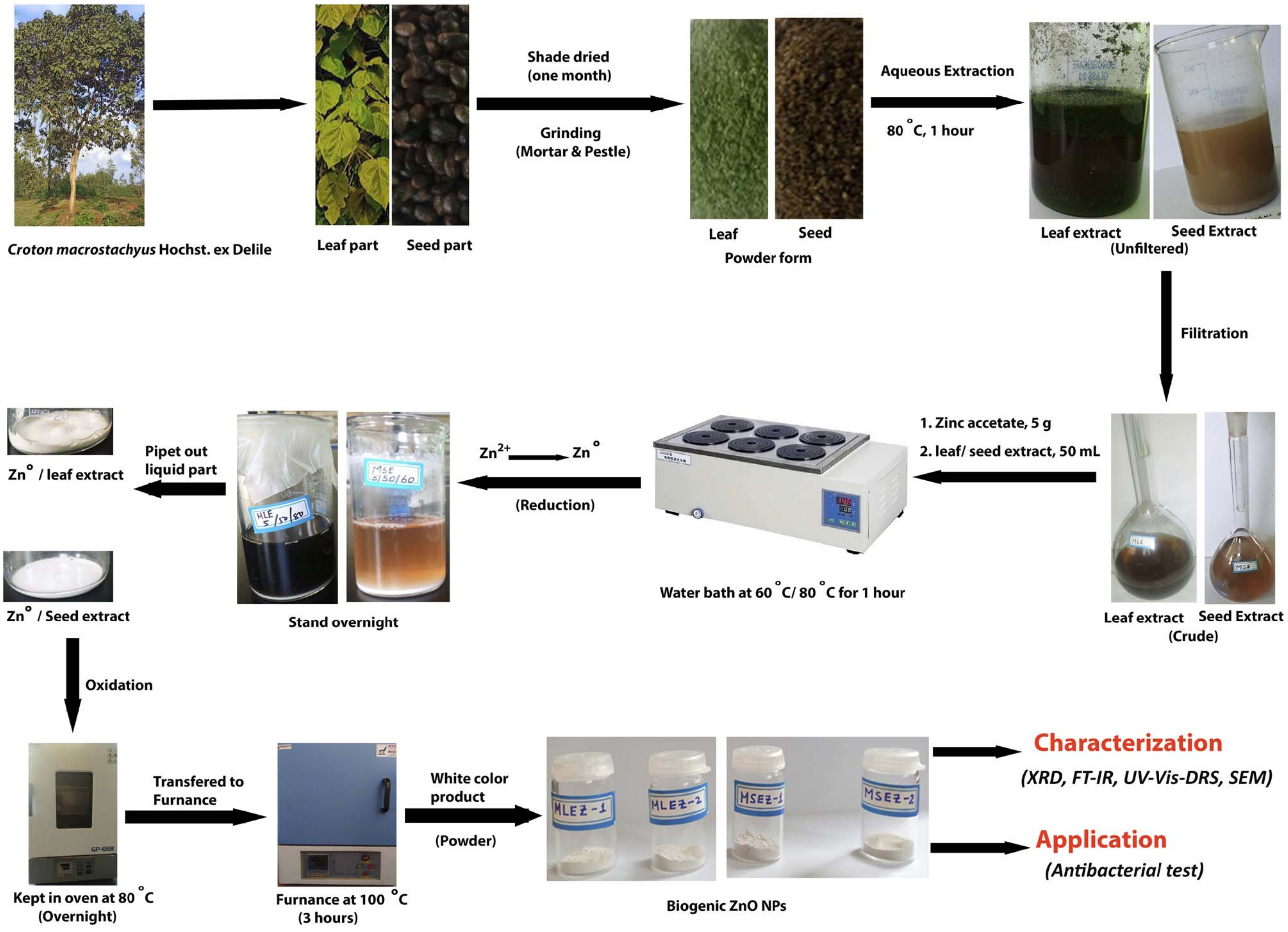

Scheme 1 Schematic representation of the synthesis of biogenic ZnO NPs.

with that of the leaf (MLE) and seed (MSE) extracts from *Croton macrostachyus* Hochst. ex Delile.

2.8 Preparation of nutrient agar

To prepare the nutrient agar, 1.38 grams of general medium was dissolved in 60 mL of distilled water. The mixture was then autoclaved at 121 °C for 15 minutes. Subsequent to autoclaving, the media was portioned into three different Petri dishes containing 20 mL of nutrient agar. Then after, using this media the bacterial strains (*S. aureus*, *K. pneumoniae*, and *P. aeruginosa*) were activated by incubating at 37 °C for 24 hours.

2.9 Preparation of ZnO NPs and crude extracts for antimicrobial testing on Mueller–Hinton agar

Mueller–Hinton Agar (MHA), 9.13 grams was dissolved in 240 mL of distilled water and subsequently autoclaved at 121 °C for 15 minutes. After cooling, 20 mL of the solution was dispensed into each of twelve Petri dishes. 1 mL of DMSO was utilized to dissolve and prepare three different concentrations of MLEZ-2 (ZnO NPs synthesized using *Croton macrostachyus* Hochst. ex Delile leaf extract at 80 °C) and MSEZ-2 (ZnO NPs synthesized using *Croton macrostachyus* Hochst. ex Delile seed extract at 80 °C). The concentrations used were 10, 20, and 40 μg mL^{-1}. In addition, leaf crude extract (MLE) and seed crude extract (MSE) were also prepared at the same concentrations. This was followed by mixing of the solutions using the vortex mixer (Model: XH.B).

2.10 Agar well diffusion assay for antibacterial activity of ZnO nanoparticles and controls

Three tubes were filled with 5 mL of saline solution and were individually inoculated with one of three bacterial strains: two Gram-negative and one Gram-positive. Wells were created in the agar plates and loaded with 10 μg mL^{-1}, 20 μg mL^{-1}, and 40 μg mL^{-1} of MLEZ-2 and MSEZ-2 ZnO nanoparticles, DMSO (negative control), and gentamicin (positive control) with a concentration of 10 μg mL^{-1} in the center. Wells with diameters of approximately 6 mm were created aseptically using sterile micropipette tips on the agar plates. The MHA plates were incubated at 37 °C for 24 hours.

2.11 Assessment of antibacterial efficacy *via* zone of inhibition

After incubation, any resulting clear zones (zones of inhibition) around the wells were measured in millimeters (mm). The agar well diffusion experiment was performed in triplicate to ensure consistency. The diameters of the inhibition zone were measured, which determined the extent of antimicrobial

Table 1 Phytochemical constituents of *Croton macrostachyus* Hochst. ex Delile leaf and seed extracts[a]

No	Constituents	Chemical test	Observation	Types of extracts	
				MLE	MSE
1	Phenolics/tannins	Ferric chloride	Blue-black or blue-green color	+	+
2	Flavonoids	Lead acetate	Yellow-orange color	+	−
3	Saponins	Froth test	Stable foam	+	+
4	Steroids	Liebermann	Upper layer turned red; H_2SO_4 layer yellow with green fluorescence	+	+
5	Terpenoids	Salkowski	Reddish-brown color	+	+
6	Alkaloids	Hager's reagent	Orange precipitate formation	+	+

[a] MLE = *Croton macrostachyus* Hochst. ex Delile plant leaf extract; MSE = *Croton macrostachyus* Hochst. ex Delile plant seed extract; + sign indicates secondary metabolite is present and − sign indicates secondary metabolite is absence.

activity. Comparisons were made with standard drugs, and the zone of inhibition was recorded in millimeters.

2.12 Determination of minimum inhibitory concentration (MIC)

The minimum inhibitory concentrations (MICs) were assessed by the broth dilution technique as explained in a previous study,[32] with minor modifications. The process began with the dissolution of 0.7 g of nutrient broth in 60 mL of distilled water and subsequent autoclaving at 121 °C for 15 minutes. The sterilized broth was then aliquoted into three sterile test tubes, each containing 20 mL.

Bacterial inocula were prepared *Staphylococcus aureus*, *Pseudomonas aeruginosa*, and *Klebsiella pneumoniae*. These strains were grown in the nutrient broth and incubated at 37 °C for 24 hours.

Separately, 2.496 g of nutrient agar was dissolved in 192 mL of distilled water and autoclaved under the same conditions. Sterile test tubes were prepared to which 2 mL of nutrient broth, 2 mL of the plant extract solution, and 0.2 μg of the bacterial inoculum were added.

The stock solutions of NPS and plant extract (MLEZ-2, MSEZ-2, MLE, and MSE) were serially diluted in the nutrient broth to give final concentrations of 50, 25, 12.5, 6.25, 3.125, and 1.56 μg mL^{-1}. Bacterial growth was checked by a visual examination of turbidity to get the MIC. The least concentration of the pure compound that showed no visible growth, displaying the absence of turbidity, was considered and recorded as the MIC.

2.13 Statistical evaluation of antimicrobial activity

The experiments were replicated thrice, and the data obtained was expressed as mean ± standard deviation (SD). Data entry and basic statistics were carried out using Microsoft Excel software. The means and standard deviations of the obtained data were computed using functions in the Excel software package. The inhibition zones of ZnO NPs and plant extracts that could inhibit the tested microorganisms were compared using one-way analysis of variance (ANOVA). Further comparison of means was done using the Least Significant Difference (LSD) Test, and the results were considered statistically significant at $p < 0.05$.

3 Results and discussions

3.1 Qualitative phytochemical screening (QPS)

Phytochemical analysis of *Croton macrostachyus* Hochst. ex Delile leaf (MLE) and seed extracts (MSE) showed the presence of a range of biological components, including phenolics, tannins, flavonoids, saponins, steroids, terpenoids, and alkaloids (Table 1). This is shown graphically in Fig. 2(a) and (b). The two extracts were found to be positive for phenolics/tannins, which gave blue-black or blue-green colorations upon the addition of a few drops of ferric chloride solution. Flavonoids were found in the leaf extract, as indicated by the formation of a yellow-orange color after treatment with a small amount of lead acetate solution, but there was no color formation in the case of the seed extract.

Both saponins and steroids were found in the extracts. This was shown using the froth test, where a persistent foam was formed. In the Liebermann–Burchard test, both extracts gave positive results. This involves a color change where the upper layer turned red and a yellow color with green fluorescence was seen in H_2SO_4. Terpenoids were also exhibited in both extracts. This was shown using the Salkowski test. This yielded a positive

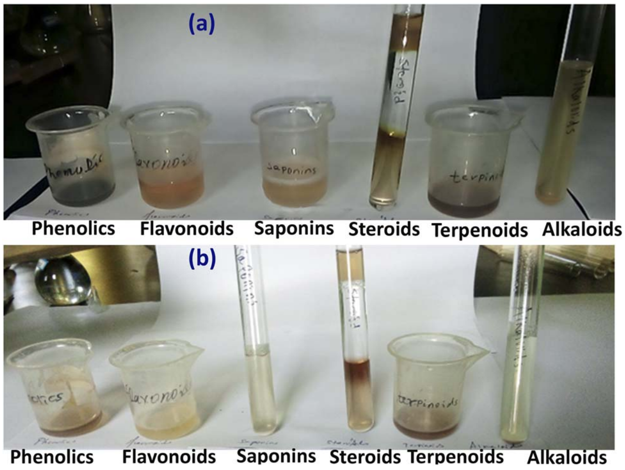

Fig. 2 Phytochemical analysis of leaf extract, MLE (a) and seed extract, MSE (b).

Table 2 Effect of metal salt loading

Loading of metal salt (g)	Volume of plant extract (mL)	Temperature (°C)	Contact time (min)	Yield (g), MLE-ZnO	Yield (g), MSE-ZnO
1.25	50	80	60	0.71	0.61
5.00	50	80	60	2.83	2.43

Table 3 Effect of plant extract volume

Loading of metal salt (g)	Volume of plant extract (mL)	Temperature (°C)	Contact time (min)	Yield (g), MLE-ZnO	Yield (g), MSE-ZnO
5.00	25	80	60	2.12	1.82
5.00	50	80	60	2.83	2.43

Table 4 Effect of contact time

Loading of metal salt (g)	Volume of plant extract (mL)	Temperature (°C)	Contact time (min)	Yield (g), MLE-ZnO	Yield (g), MSE-ZnO
5.00	50	80	30	2.26	1.94
5.00	50	80	60	2.83	2.43

result where a reddish-brown color was formed after both chloroform and concentrated sulfuric acid had been added. In both leaf and seed extracts, a positive result was shown. This was demonstrated after HCl was added as Hager's reagent formed an orange precipitate.

In this study, the extracts were utilized as natural reducing and stabilizing agents for the green synthesis of ZnO nanoparticles, highlighting their potential in eco-friendly nanomaterial preparation. The presence of these phytochemicals indicates that *C. macrostachyus* is a valuable source of secondary metabolites with pharmacological potential and can serve as a sustainable resource for nanoparticle synthesis.

3.2 Synthesis and identification of ZnO nanoparticles

Four different samples of ZnO nanoparticles have been successfully synthesized through the green method using extracts of the plant *Croton macrostachyus* Hochst. ex Delile. The samples were named MLEZ-1, MLEZ-2, MSEZ-1, and MSEZ-2 to differentiate the plant part used in the synthesis. MLEZ-1, MLEZ-2 were synthesized from MLE (leaf extract) at 60 °C and 80 °C temperatures, respectively. Similarly, MSEZ-1 & MSEZ-2 were synthesized from MSE (seed extract) at the same temperatures. This gives a clear distinction in regards to the parameters of synthesis and plant parts used in the green synthesis method.

3.3 Optimization of zinc oxide nanoparticles synthesis parameters

The optimization of zinc oxide nanoparticle (ZnO-NPs) synthesis parameters using green methods demonstrates the significant influence of precursor concentration, plant extract volume, contact time, and temperature on nanoparticle yield and quality (Tables 2–5). Each parameter plays a critical role in controlling the nucleation and growth of ZnO-NPs, ultimately affecting their physicochemical properties.

3.3.1 Effect of metal salt concentration. The quantity of zinc acetate dihydrate used as the precursor is directly proportional to the yield of ZnO-NPs produced (Table 2). Increasing the concentration of the metal salt from 1.25 g to 5 g significantly increased the yield of nanoparticle formation.

Maximum yield was found with 5 g, yielding 2.83 g of MLE-ZnO and 2.43 g of MSE-ZnO NPs under the same conditions. This is consistent with earlier research,[33] which suggests that as the availability of the precursor increases, the formation of nucleation sites will increase, thus increasing nanoparticle yields. Excessive salt levels above the optimized values may cause agglomeration, which needs be addressed in future research.

3.3.2 Effect of plant extract volume. Plant extract volume, acting as the reducing and stabilizing agents, plays a major role in the synthesis of nanoparticles. Greater volumes of the extract, ranging from 25 mL to 50 mL, showed (Table 3) better results in yield, hence the need for optimal concentrations of phytochemicals for effective reduction and stabilization of Zn ions in the reaction. Higher volumes of plant extracts contain high secondary metabolites, thus fast reaction kinetics.[34]

3.3.3 Effect of contact time. Incubation time is another parameter that is highly important for the preparation of ZnO-NPs. An increase in the contact time from 30 minutes to 1 hour led to an enhanced yield, with 1 hour being ideal for both MLE-ZnO and MSE-ZnO nanoparticles (Table 4). This is because longer contact times enable full reduction of metal ions, as well as proper crystallization of nanoparticles.[35] However, overlong incubation times may not produce better yields.

Table 5 Effect of temperature

Loading of metal salt (g)	Volume of plant extract (mL)	Temperature (°C)	Contact time (min)	Yield (g), MLE-ZnO	Yield (g), MSE-ZnO
5.00	50	60	60	2.63	2.00
5.00	50	80	60	2.83	2.43

3.3.4 Effect of temperature. Temperature is one of the factors that are important for the activation of biological molecules and hence facilitates an increase in the rate of reactions.

The findings highlighted that when the synthesis process is carried out at 80 °C, the yields are higher (Table 5) compared to 60 °C, which can be attributed to efficient activation of phytochemicals.[36] Though increased temperatures are preferred for manufacturing nanophased particles, finer temperatures are required for activating biological compounds.

3.3.5 Overall optimization. The combined contribution of these factors suggests that the optimal conditions for the green synthesis of ZnO-NPs are 5 g of Zn acetate dihydrate, 50 mL of the extract, a 1 h contact time, and a temperature of 80 °C. Using the aforementioned optimal parameters for the green synthesis of ZnO-NPs resulted in the maximum yield of MLE-ZnO-NPs (2.83 g) and MSE-ZnO-NPs (2.43 g).

3.4 Characterization of ZnO NPs

3.4.1 PXRD analysis and structural characterization. The XRD patterns of all synthesized ZnO nanoparticles, such as MLEZ-1, MLEZ-2, MSEZ-1, and MSEZ-2, are displayed in Fig. 3. These samples were prepared using *Croton macrostachyus* Hochst. ex Delile leaf and seed extracts at two different temperatures, 60 °C and 80 °C. The diffraction profile of all samples shows a sharp and well-defined peak, which proves the development of highly crystalline ZnO nanoparticles. The observed reflections correspond to the hexagonal wurtzite structure of ZnO, validated by the standard reference card JCPDS 00-036-1451 and crystallographic data CCDC 1481937, assigning the material to the $P6_3mc$ space group.

The major peaks observed at 2θ values of 31.7°, 34.4°, and 36.2° were assignable to the (100), (002), and (101) planes, respectively. Of these, the (002) peak at 34.4° had the sharpest peak, indicating a preferred orientation in the *c*-axis. Other distinctive peaks were observed at 47.5°, 56.6°, 62.8°, and 68.0°, which corresponded to the (102), $(2\bar{1}0)$, (103), and $(2\bar{1}2)$ planes, respectively. Sharpness and high intensity of these reflections confirmed the successful formation of ZnO nanoparticles.

Notably, two small peaks appeared at 29.46° and 30.96°, which are not from the ZnO pattern. These were indexed as the (104) planes of calcite ($CaCO_3$)[37] and dolomite ($CaMg(CO_3)_2$),[38] respectively. This result is in agreement with the XPS result, which showed the presence of Ca and Mg in the specimens. These components may arise from the phytochemicals or mineral contents of the plant materials used in the green method of synthesis. Due to its small intensity, this carbonate form is only present in trace amounts, either as residues or as weakly bound components to the ZnO NPs.

Overall, the PXRD analysis confirms that the major material synthesized is high-crystallinity hexagonal wurtzite ZnO nanoparticles, confirmed by both JCPDS and CCDC references. The minor peaks recorded indicate the presence of calcium- and magnesium-based carbonate phases, which would be expected for green synthesis due to natural precursors emanating from the plant extract. This idea is further supported by XPS, detecting Ca and Mg that might well be present as surface species, dopants, or even small carbonate residues. Together, PXRD and XPS yield a consistent view that the material is principally composed of ZnO nanoparticles with trace

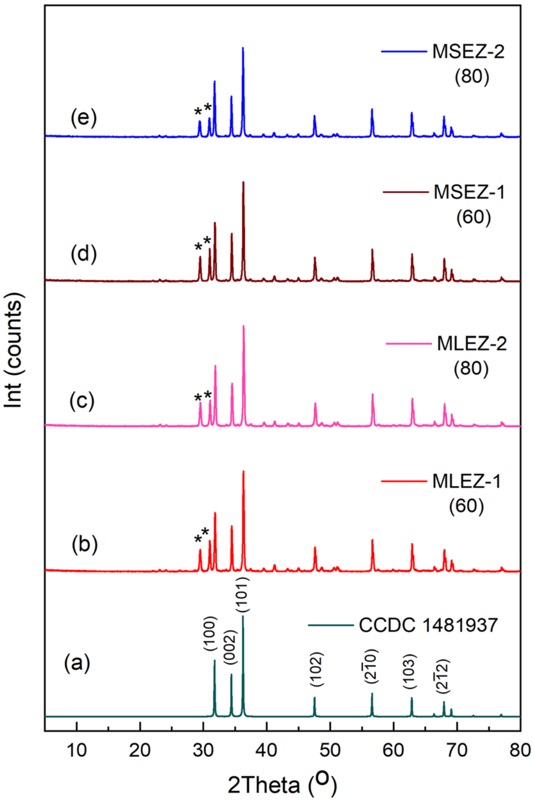

Fig. 3 XRD patterns of ZnO nanoparticles: (a) calculated from CIFs in CCDC 1481937; (b) biosynthesized ZnO NPs using leaf extracts (MLEZ-1) at 60 °C; (c) biosynthesized ZnO NPs using leaf extracts (MLEZ-2) at 80 °C; (d) biosynthesized ZnO NPs using seed extracts (MSEZ-1) at 60 °C; and (e) biosynthesized ZnO NPs using seed extracts (MSEZ-2) at 80 °C from the *Croton macrostachyus* Hochst. ex Delile plant.

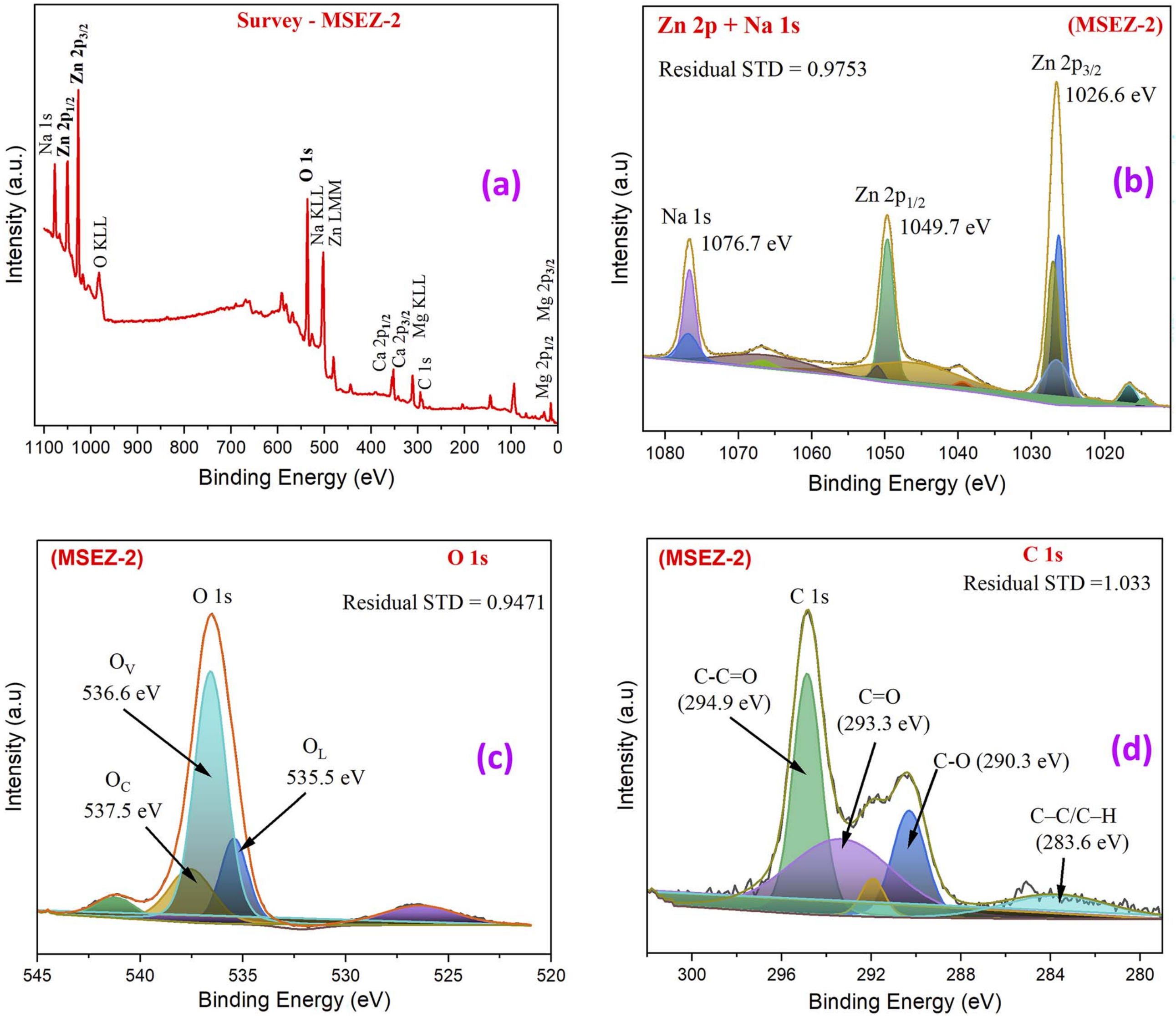

Fig. 4 Wide-scan XPS survey spectrum (a); XPS spectrum of Zn 2p (b); XPS spectrum of O 1s (c); XPS spectrum of C 1s (d) of MSEZ-2.

contributions from Ca and Mg, reflecting both the structural integrity of ZnO and the biological synthesis route.

3.4.2 Crystallite size analysis of biosynthesized ZnO nanoparticles.

The average crystallite size (ACS) of the biosynthesized ZnO nanoparticles was calculated using the Debye–Scherrer formula, as it was difficult for us to obtain higher resolution SEM or TEM images. We recognize that this is only a rough estimate of the crystallite size and does not take into account various factors such as lattice strain or agglomeration. This equation depends upon the XRD data, indicating broadening of XRD peaks for nanoparticles. The formula can be represented as:

$$D = \frac{(k \times \lambda)}{\beta \times \cos \theta}$$

where: $k = 0.94$ (Scherrer constant), $\lambda = 1.54056$ Å (wavelength of X-ray), $\beta =$ FWHM of diffraction peak, and $\theta =$ Bragg angle. The crystallite size was measured in the five strongest XRD peaks for every sample and is depicted in Table S1. The calculated average size was 41.40 nm for MSEZ-2, 42.00 nm for MSEZ-1, 40.28 nm for MLEZ-2, and 41.16 nm for MLEZ-1. It is evident that the prepared ZnO NPs are in the nanoscale range (0–100 nm), showing good crystallinity as indicated by prominent diffraction peaks.

Temperature played an important role in particle size variation. Among various conditions studied, 80 °C is found to be optimal for the synthesis of ZnO NPs with smaller crystallites (MSEZ-2 and MLEZ-2) than those obtained under other conditions. This finding is supported by previous studies,[39,40] which found that increased temperatures increase the rate of reduction of zinc ions and their nucleation, thus forming smaller particles. Higher temperatures increase the dispersal of zinc ions to form nuclei because of the increase in the rate of reduction of zinc ions.

The smaller crystallites formed under optimum conditions are more significant because they are directly linked to enhanced antibacterial activity. This is expected because previously, smaller particle sizes were found to produce higher antimicrobial activity due to increased surface reactivity.[40] Once again, the findings here confirm that by appropriately adjusting synthesis variables such as temperature and using the correct extracts, ZnO nanoparticles can be synthesized for specific applications.

3.4.3 XPS analysis of biosynthesized ZnO-NPs. X-Ray Photoelectron Spectroscopy (XPS) analysis was used to interpret the surface chemical compositions and oxidation states of biogenically synthesized ZnO NPs using zinc acetate and leaf/seed extracts of *Croton macrostachyus* Hochst. ex Delile. XPS is an important tool for interpreting the nanoparticle surface composition at an atomic level, which is fundamental for determining any potential nanoparticle applications.[41]

The survey scan and the high-resolution spectra verify the presence of Zn, O, and C, which is expected in the presence of ZnO NPs. There are also traces of Na, as expected from the synthesis procedure and the use of plant stabilizers. Notably, the existence of Mg and Ca ions from the plant extracts is identified through the XPS survey scan spectra (Fig. 4a and 5a). These ions appear in the form of distinctive peaks in the Ca 2p or Mg 2p regions. This suggests the presence of these ions on the surface of the nanoparticle due to the biogenic synthesis process.[42,43] The incorporation of these minor elements (Na, Mg, and Ca) can influence the surface chemistry and functional properties of ZnO NPs.[44–46] For instance, Mg and Ca ions may contribute to surface charge modulation, defect formation, and potential catalytic or biological activity enhancement. Their presence highlights the complexity and richness of biogenic synthesis routes, where plant extracts act not only as reducing and stabilizing agents but also as sources of additional elemental species that can tailor nanoparticle properties.

3.4.3.1 Zinc (Zn 2p) spectrum. The Zn 2p core-level spectra (Fig. 4b and 5b) display two prominent peaks at binding energies of 1026 eV (Zn $2p_{3/2}$) and 1049 eV (Zn $2p_{1/2}$), with a spin–

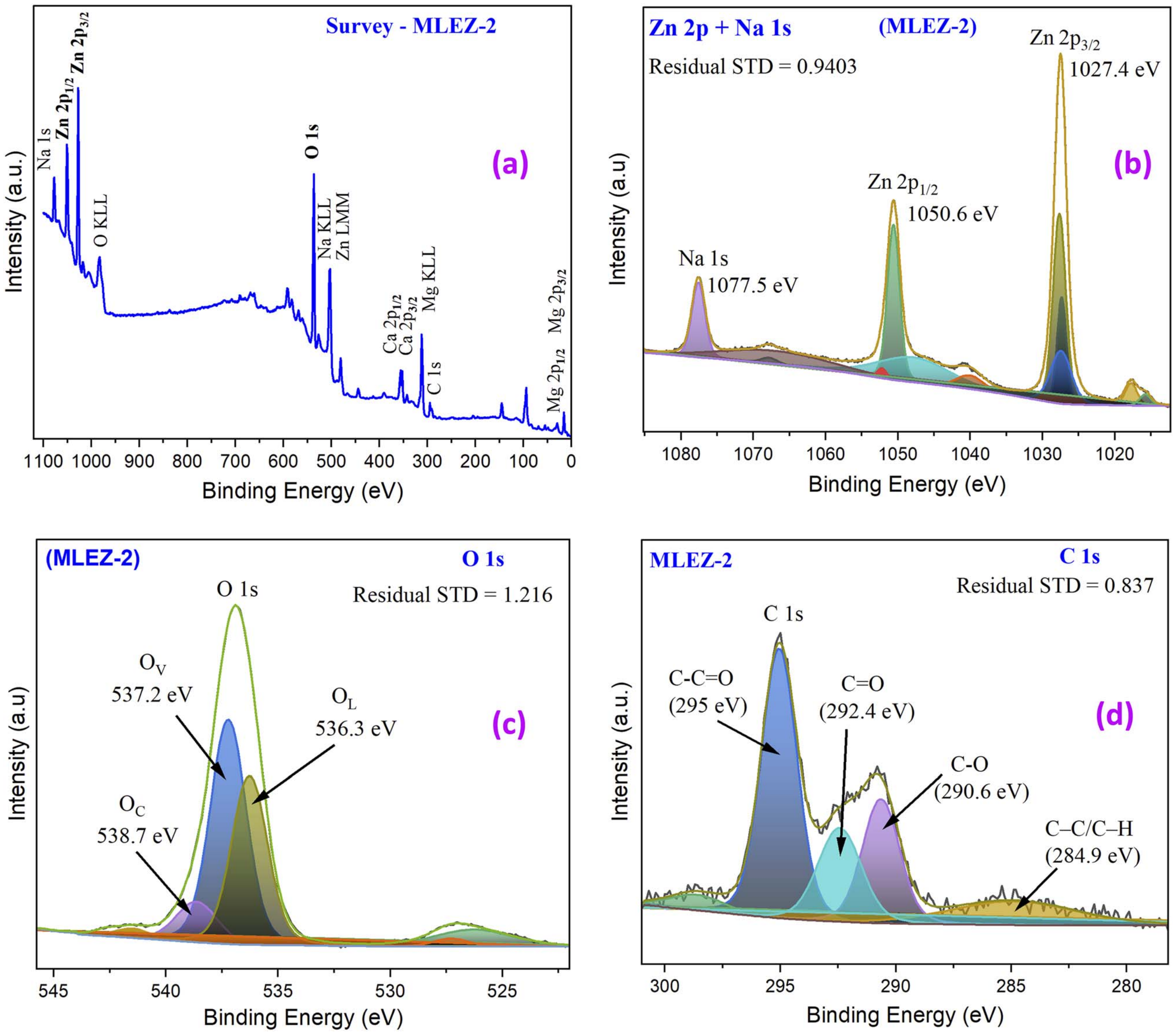

Fig. 5 Wide-scan XPS survey spectrum (a); XPS spectrum of Zn 2p (b); XPS spectrum of O 1s (c); XPS spectrum of C 1s (d) of MLEZ-2.

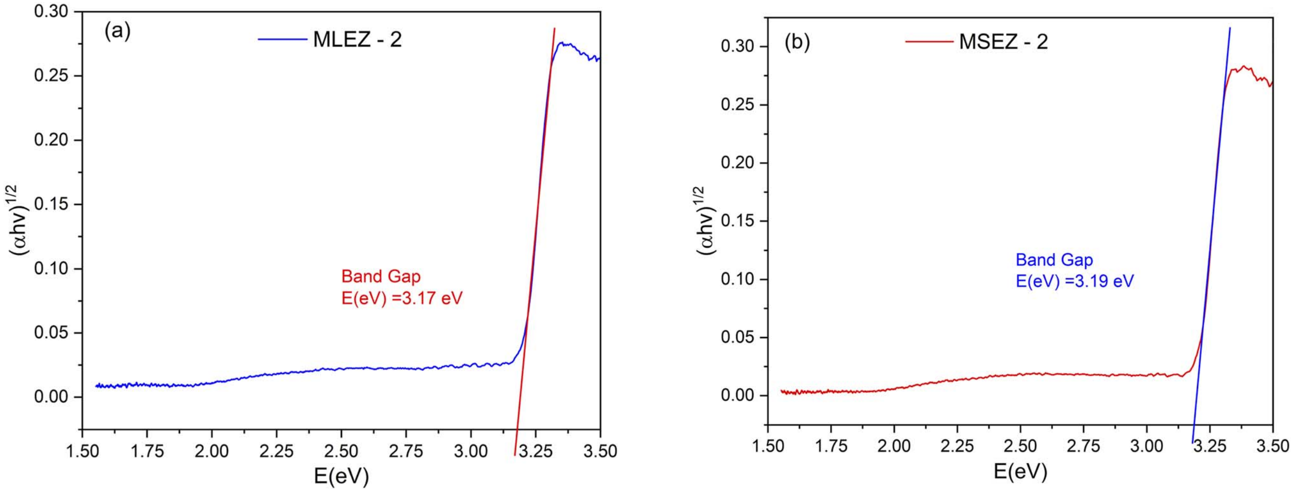

Fig. 6 Tauc plot for ZnO NPs (MLEZ-2) prepared from leaf extract (a); Tauc plot for ZnO NPs (MSEZ-2) prepared from leaf extract (b).

orbit splitting of about 23 eV, characteristic of Zn^{2+} ions in ZnO (MSEZ-2 & MLEZ-2). The lack of other peaks related to metallic zinc or zinc hydroxides in the spectrum ensures the completeness of oxidation in biogenesis. The smaller peak at 1076 eV for Na 1s is indicative of sodium ions remaining in plant extracts or washing procedures and do not affect zinc oxide formation but could impact charge and dispersibility.

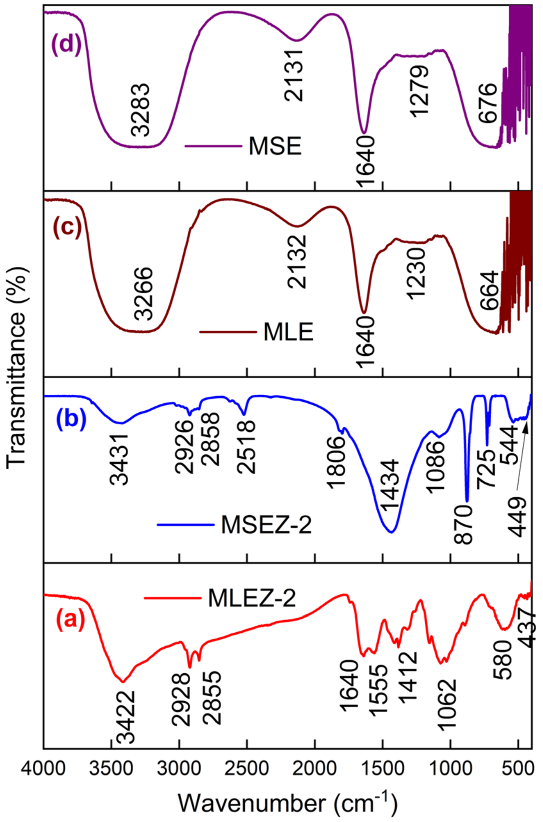

Fig. 7 FTIR spectra of *Croton macrostachyus* Hochst. ex Delile extracts and their respective ZnO nanoparticles: (a) ZnO nanoparticles synthesized using leaf extract (MLEZ-2), (b) ZnO nanoparticles synthesized using seed extract (MSEZ-2), (c) leaf extract (MLE), and (d) seed extract (MSE). The spectra illustrate characteristic functional groups present in the extracts and confirm their interaction with ZnO nanoparticles.

3.4.3.2 Oxygen (O 1s) spectrum. The high-resolution O 1s spectra of the MSEZ-2 and MLEZ-2 samples (Fig. 4c and 5c) allow for the identification of multiple oxygen species present within the surface chemistry of ZnO nanoparticles. The major peak at about 535 eV is attributed to the presence of lattice oxygen (O_L), denoting O^{2-} present within the ZnO lattice. Besides this major peak, other oxygen species including oxygen vacancies (O_V), denoted by a peak at about 536 eV, are also present. A main characteristic defect is denoted by a peak at 537 eV for a chemisorbed oxygen species (O_C), denoted by O^- or O^{2-} present on the ZnO surface.[44] These highly reactive oxygen species are responsible for affecting the antimicrobial and photocatalytic behaviours. The presence of oxygen vacancies alongside the other oxygen species tends to produce a defect-rich surface. The co-existence of the major oxygen species, including oxygen vacancies as well as the corresponding chemisorbed oxygen species, manifests the importance of defect engineering in the production of ZnO for enhanced functional applications.

3.4.3.3 Carbon (C 1s) spectrum. The C 1s spectrum in high resolution shows several deconvoluted peaks, representing different carbon species (Fig. 4d and 5d). The most dominant peak occurring at about 284 eV is due to C–C/C–H bonds, which normally arise from adventitious carbon or organic compounds from the plant extract. The peaks occurring at around 290 eV, 293 eV, and 294.9 eV are assigned to C–O, C═O, and C–C═O functional groups, respectively, typical of polyphenols, flavonoids, and other biomolecules present in *C. macrostachyus*.[47] These functional groups confirm the successful capping of ZnO NPs by phytochemicals, which play a dual role as reducing agents and stabilizers during nanoparticle formation. Such surface functionalization is advantageous for improving colloidal stability and imparting bioactivity.

XPS spectra verify the successful biogenic synthesis of ZnO nanoparticles with a major composition of Zn^{2+} and O^{2-} ions along with the adsorption of organic compounds on the surface of ZnO using the phytoextracts of *C. macrostachyus*. Identification of peaks for C–O bonds along with peaks for C═O bonds reveals the successful capping of the biogenically synthesized ZnO nanostructures using phytoextracts for improving dispersion forces and suppressing agglomeration phenomena. These phytoextract-mediated biogenic nanostructures ensure purity along with imparting biological properties with potential utility for increasing the efficacy of ZnO nanostructures toward biomedical, photocatalytic, and other applications. Additionally, the observed peaks for the presence of hydroxyl groups along with organic compounds might aid in further modifying these nanostructures for target-specific antimicrobial activities.

3.4.4 Optical band gap determination. The optical properties of biogeneically synthesized ZnO NPs using leaf and seed extracts of *Croton macrostachyus* Hochst. ex Delile were analyzed using the Tauc plot technique. Fig. 6a is indicative of the Tauc plots of leaf extract-based ZnO NPs (MLEZ-2), whereas Fig. 6b is indicative of seed extract-based ZnO NPs (MSEZ-2). The band gap energy was determined by extrapolating the linear portion of the $(\alpha h\nu)^{1/2}$ *versus* photon energy (E) curve to the energy axis. The calculated band gap values were 3.17 eV for MLEZ-2 and 3.19 eV for MSEZ-2.

These values are slightly lower than the bulk ZnO[48] band gap (3.37 eV), which is typical for nanoscale ZnO due to the influence of surface defects and organic molecules from the plant extract. The small difference in values between the two samples is probably due to differences in phytochemical compositions of leaf and seed extracts affected by nanoparticles formation processes such as nucleation and growth mechanisms. The extracts contain natural molecules that could lead to defects in the nanoparticles as well as affect its surface chemistry in creating defects in its crystallinity and band gap energy of nanoparticles due to quantum confinement effects observed in small particles like nanoparticles. When compared with the literature, the band gaps determined in the present study (3.17–3.19 eV) match ZnO NPs prepared by green techniques. For instance, ZnO NPs prepared by *Aloe vera* extract[49] had band gaps in the range 3.20–3.25 eV, and ZnO NPs prepared by *Moringa oleifera* seed extract[50] had a band gap energy of 3.18 eV. Similarly, ZnO nanoparticles synthesized from *Azadirachta indica* extract[51] have been found to have band gaps ranging from 3.21 eV to 3.26 eV. However, generally, ZnO nanoparticles synthesized by the chemical method have band gaps from 3.20 eV to 3.30 eV based on their size and synthesis methodology. Although the band gap of the prepared ZnO NPs is smaller than that of the bulk material, it indicates that there are defect levels introduced during the biogenic synthesis due to the biomolecules. These defect levels can increase the absorbability of visible light, thus paving the way for their use in optoelectronics and photocatalysis.

Thus, in general, the obtained results validate that biogenic synthesis by extraction of *Croton macrostachyus* Hochst. ex Delile leaves leads to ZnO nanoparticles that have optical similarities in comparison to the ones obtained by various biogenic routes.

3.4.5 FTIR analysis of biosynthesis ZnO NPs. The FTIR spectra of *Croton macrostachyus* Hochst. ex Delile leaf extract, MLE; seed extract, MSE, and their corresponding ZnO nanoparticles, MLEZ-2 and MSEZ-2, are shown in Fig. 7 and Table S2.

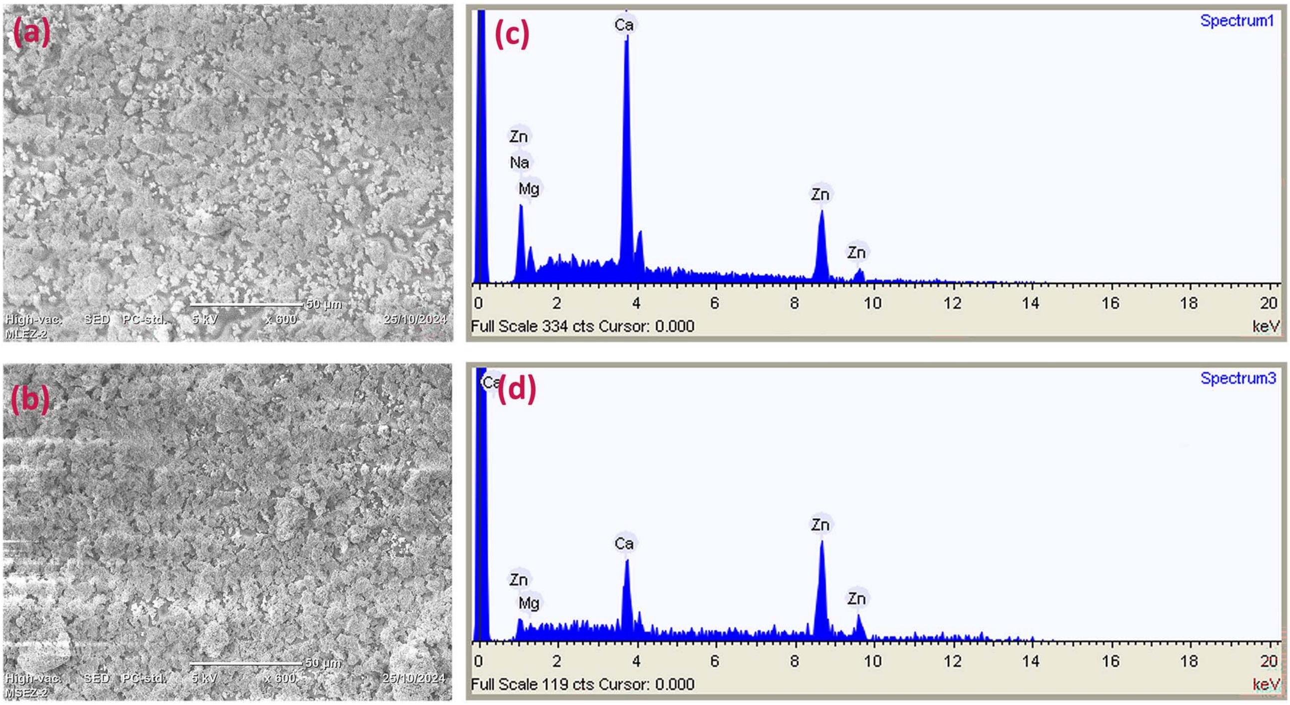

Fig. 8 (a) SEM image of MLEZ-2; (b) SEM image of MSEZ-2; (c) EDS spectrum for MLEZ-2; (d) EDS spectrum for MSEZ-2 of the biosynthesized ZnO NPs by *Croton macrostachyus* Hochst ex Delile.

The extracts (Fig. 7c and d) showed broad absorption bands at 3266 cm^{-1} and 3283 cm^{-1}, which can be assigned to O–H stretching vibrations of hydroxyl groups for MLE and MSE, respectively, indicating the presence of alcohols and phenolic compounds.[52] Peaks observed at 2132–2131 cm^{-1} are attributed to C≡C stretching of alkynes, while strong absorption at 1640 cm^{-1} represents C═O stretching of amide or carbonyl groups, suggesting proteins or other carbonyl-containing biomolecules.[53] Additional bands at 1230–1279 cm^{-1} indicate C–O stretching of esters or phenolic groups, and the peaks near 664–676 cm^{-1} correspond to aromatic ring bending vibrations. These functional groups confirm that the extracts contain polyphenols, proteins, and other biomolecules that can act as reducing and capping agents during ZnO nanoparticle synthesis.[52]

However, the FTIR spectra of the biosynthesized ZnO nanoparticles (MLEZ-2 and MSEZ-2) in Fig. 7a and b demonstrate clear peaks ranging from 449–580 cm^{-1} corresponding to the Zn–O vibration of ZnO. The broad peak of 3422 cm^{-1} in Fig. 7a indicates the existence of O–H bonds in MLEZ-2. The other peaks of 2928 and 2855 cm^{-1} in Fig. 7a represent C–H bonds of aliphatic groups, which suggest the existence of organic material on the surface of the ZnO nanoparticles. Peaks at 1640, 1555, and 1412 cm^{-1} are associated with amide and carboxylate groups, indicating protein involvement in stabilization. Similarly, MSEZ-2 exhibits features at 3431 cm^{-1} (O–H), 2926–2858 cm^{-1} (C–H), and 1434 cm^{-1} (carboxylate), along with Zn–O bands at 449, 544, and 725 cm^{-1}.[52] The absence or diminution in some of the peak intensities, for instance 2131–2132 cm^{-1}, in the spectra of the nanoparticles suggests that these groups took part in the reduction process of Zn^{2+} ions for the production of the nanoparticles.

In general, the FTIR analysis supports the fact that phytochemical constituents of the *Croton macrostachyus* Hochst. ex Delile extracts, such as phenols, proteins, and carboxylates, act as dual agents of reduction and capping in the biosynthesis of the ZnO NPs. The presence of the Zn–O bond in the fingerprint region of the FTIR-spectrum is sufficient proof of the successful fabrication of the NPs, in addition to the presence of the functional group of the phytochemical constituent on the surface of the NPs.

3.4.6 Morphological and elemental analysis. SEM analyses of ZnO nanoparticles prepared using *Croton macrostachyus* Hochst. ex Delile leaf (MLEZ-2) and seed (MSEZ-2) extracts show aggregated clusters that are irregular with rough surfaces, a characteristic typical of plant-mediated synthesis. However, MLEZ-2 (Fig. 8a) gives more granular domains than MSEZ-2, which forms denser film-like structures (Fig. 8b), indicating some compositional differences between the leaf and seed extracts.[54] The EDS spectra of the biogenic ZnO nanoparticles (Fig. 8c and d) reveal high intensities of Zn, thus verifying that Zn is the major component, whereas the presence of small amounts of Na, Mg, and Ca should be considered with caution since EDS is a surface sensitive and semi quantitative technique. The higher intensity of Ca may be attributed to the surface enrichment of plant metabolites. This conclusion is also supported by the XPS data (Fig. 4 and 5), which indicate that Zn is the major component and Na^{+}, Mg^{2+}, and Ca^{2+} are present in trace amounts. The particle aggregation is mainly attributed to the presence of surface-bound organic functional groups and biogenic residues, whereas the trace amounts of inorganic ions contribute very little to the aggregation. While oxygen and carbon have less distinct peaks in EDS measurements owing to low-energy interactions, their presence was confirmed by XPS measurements (Fig. 4 and 5).[54,55] XPS measurements in Fig. 4b and 5b confirmed these observations. They revealed zinc species in ZnO (Zn 2p peaks), oxygen in the lattice or surface hydroxyl groups (O 1s), and carbon in phytochemical materials (C 1s).

Taken together, the results of SEM, EDS, and XPS analyses indicate that purely ZnO nanoparticles are biosynthetically composed of ZnO. Among others, the bio-functional surfaces are rich in organic functional groups and minute amounts of inorganic ions. The latter materials tend to affect their morphology and applications.

3.5 Antibacterial activity of biosynthesized ZnO nanoparticles and crude extracts

The biosynthesised zinc oxide nanoparticles (ZnO NPs) from *Croton macrostachyus* Hochst. ex Delile leaf and seed extracts (MLEZ-2 and MSEZ-2), were screened for their antibacterial activities using the agar well diffusion method against *Staphylococcus aureus*, *Pseudomonas aeruginosa,* and *Klebsiella pneumoniae* bacterial strains. Zone of inhibition was measured at three concentrations (10, 20, and 40 μg mL^{-1}), and results are depicted in Fig. 9, Fig. 10, and Table S3. The synthesized ZnO NPs showed very promising antibacterial activity, which increases with concentration.

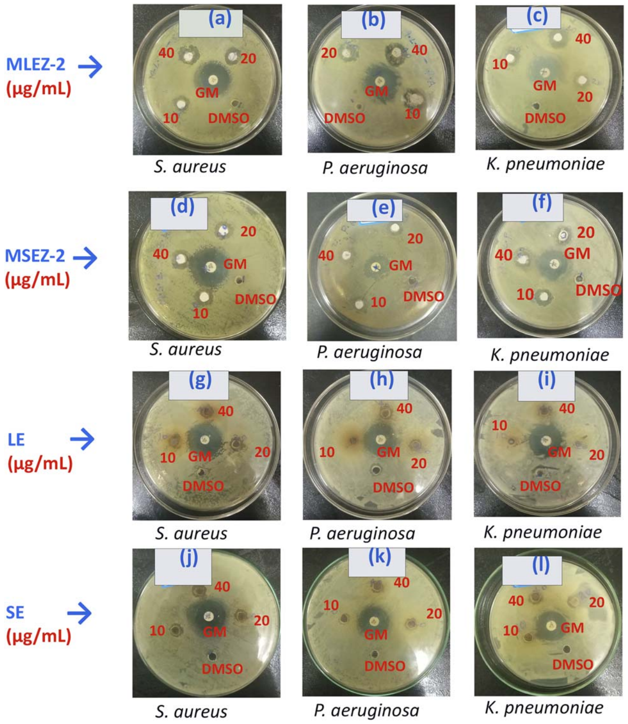

Fig. 9 Agar well diffusion assay showing the effect of different concentrations of NPs, LE, and SE against bacterial strains: (a, d, g and j) *S. aureus*, (b, e, h and k) *P. aeruginosa*, and (c, f, i and l) *K. pneumoniae*.

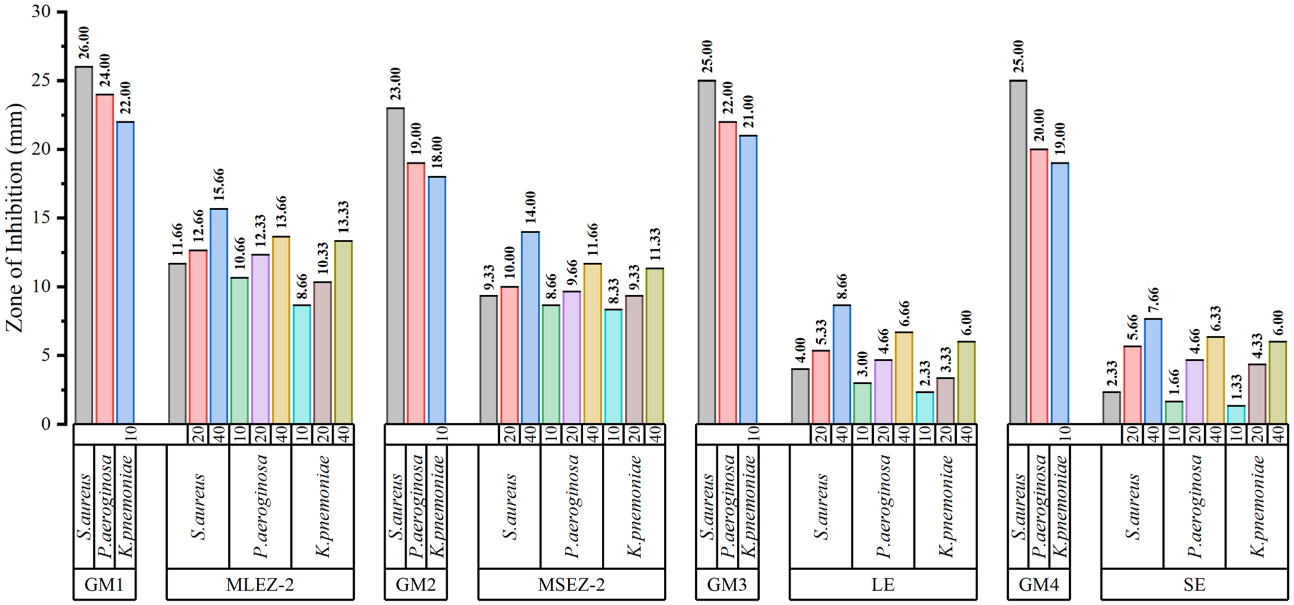

Fig. 10 Mean ± SD clustered column charts showing antibacterial activities of ZnO nanoparticles (MLEZ-2 and MSEZ-2) and crude extracts (LE and SE), compared with the positive control (GM).

For MLEZ-2 ZnO NPs, inhibition zones against *S. aureus* increased from 11.66 ± 0.94 mm at 10 μg mL^{-1} to 15.66 ± 0.47 mm at 40 μg mL^{-1}. Similarly, *P. aeruginosa* showed an increase from 10.66 ± 0.47 mm to 13.66 ± 0.47 mm, and *K. pneumoniae* from 8.66 ± 0.47 mm to 13.33 ± 0.47 mm across the same concentration range.

MSEZ-2 ZnO NPs followed the same trend but gave slightly lower inhibition values compared to MLEZ-2. LE and SE crude extracts exhibited poor antibacterial activity as compared to ZnO NPs, with LE giving the maximum inhibition zone of 8.66 ± 0.47 mm against *S. aureus* and SE giving 7.66 ± 0.47 mm at 40 μg mL^{-1}. In contrast, the positive control gentamicin (10 μg mL^{-1}) gave inhibition zones of 22–26 mm, whereas the negative control DMSO presented no activity. The above results confirm that antibacterial activity is dose dependent and ZnO NPs synthesized through a green synthesis route exhibits better antibacterial action than crude plant extracts alone.

The antibacterial activity of ZnO NPs was found to be more against Gram-positive bacteria *S. aureus* in comparison to Gram-negative bacteria (*P. aeruginosa* and *K. pneumoniae*). This result is in accordance with past research,[56] where the reason is explained to be the variation in the cell wall of the bacteria. Gram-positive bacteria have thicker peptidoglycans, which help in the interaction of the zinc oxide NPs, whereas Gram-negative bacteria have an outer membrane that protects against NPs.[57] Thus, the antibacterial effect of ZnO NPs is more pronounced against Gram-positive bacteria. The major reason for the increased antibacterial properties of ZnO NPs is their capacity to produce reactive oxygen species (ROS) like H_2O_2, which can easily enter the bacterial cell membrane, leading to death.[58] The smaller size of ZnO NPs, with their larger surface area, leads to an increased ability to generate ROS, hence their high bactericidal properties.[59] The method of green synthesis used in the study could be responsible for the high antibacterial properties exhibited. Furthermore, the dissolution of Zn^{2+} ions from the nanoparticles and the subsequent formation of H_2O_2 molecules further enhance their antibacterial action. A report has confirmed that smaller particle size increases antibacterial efficacy due to greater surface area and higher concentrations of reactive oxygen species.[60] The suggested antibacterial mechanism *via* ROS is theoretical and relies upon literature reports.

The differences observed among ZnO NPs, crude extracts, and controls for antibacterial activity were statistically significant at a level of significance of 0.05 using LSD post-hoc tests. This further verifies that biosynthesized ZnO NPs have more antibacterial activity than crude extracts and are effective against both Gram positive and Gram negative bacteria, but more effective against Gram positive bacteria. From the above observations, it has been revealed that ZnO NPs synthesized by the extracts of *Croton macrostachyus* Hochst. ex Delile have potential usage as antibacterial agents against Gram-positive bacteria.

3.6 Minimum inhibition concentration

The antibacterial potency of zinc oxide nanoparticles (ZnO NPs) prepared by biosynthesis using leaf and seed extracts of *Croton macrostachyus* Hochst. ex Delile was tested by the Minimum Inhibitory Concentration (MIC) method. According to

Table 6 MIC of MLEZ-2 and MSEZ-2 ZnO NPs and leaf and seed crude extracts of *Croton macrostachyus* Hochst. ex Delile against pathogenic bacteria

	Minimum inhibition concentration (μg mL^{-1})			
Bacteria strain	MLEZ-2	MSEZ-2	LE	SE
S. aureus	3.125	3.125	6.25	6.25
P. aeroginosa	3.125	6.25	12.5	12.5
K. pnemoniae	6.25	3.125	6.25	25.0

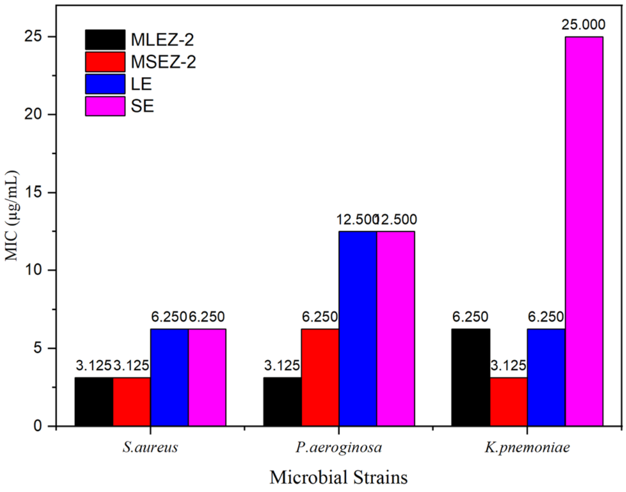

Fig. 11 Bar graph showing the minimum inhibitory concentrations (MIC) of biosynthesized ZnO nanoparticles (MLEZ-2 and MSEZ-2) and crude extracts (LE and SE) against pathogenic bacteria.

definition, MIC is the "smallest concentration, in micrograms or milligrams per milliliter, giving complete inhibition of visible growth by a test organism under controlled conditions in an *in vitro* test system."[61]

In the current study, the value of MIC could range from 50 µg mL^{-1} to 1.56 µg mL^{-1}. The determination of MIC was essential to identify the lowest concentration of ZnO NPs capable of inhibiting bacterial growth. Table 6 summarizes the MIC values for biosynthesized ZnO NPs (MLEZ-2 and MSEZ-2) and crude extracts (LE and SE) against three pathogenic bacteria: *Staphylococcus aureus*, *Pseudomonas aeruginosa*, and *Klebsiella pneumoniae*.

The result shows that ZnO NPs prepared using leaf and seed extracts have significantly lower MIC values than the crude extracts, displaying greater antibacterial potential. The result corroborates earlier research, which suggested that green synthesis of ZnO NPs has an MIC value of 1–4 µg mL^{-1} for *S. aureus* and *P. aeruginosa*.[62]

The lowest MIC value obtained (3.125 µg mL^{-1}) for *S. aureus* by MLEZ-2 and MSEZ-2 ZnO NPs clearly shows their effective inhibitory action in lower concentrations. According to previous research, comparable mic values range from 1.87 to 3.12 µg mL^{-1} for such bacterial strains.[62]

P. aeruginosa and *K. pneumoniae* were effectively inhibited by MIC values ranging from 3.125–6.25 µg mL^{-1} for ZnO NPs, whereas crude extracts required higher concentrations (6.25–25 µg mL^{-1}), in line with broader reports showing ZnO NP MICs within the µg mL^{-1} to mg mL^{-1} range for Gram-negative bacteria.[63] Fig. 11 illustrates the dose-dependent increase in inhibition zones as ZnO NP concentration increases, supporting the typical pattern of MIC-defined antimicrobial activity. Very low concentrations (<1.56 µg mL^{-1}) did not exhibit antibacterial activity. This could be due to the fact that a concentration below the MIC may serve as a nutrient source for bacteria, which may result in increased growth of bacteria, as it has been observed in previous studies on ZnO nanoparticles.[64]

Thus, it is clear that low MIC values for ZnO NPs indicate their potential to serve as strong antimicrobial agents. The MIC value of 25 µg mL^{-1} for *K. pneumoniae* using seed crude extract (SE) further strengthens the idea of low effectiveness of unprocessed extracts. The considerable improvement in antimicrobial property by reducing it to NPs reveals further research potential of ZnO NPs in antimicrobial research.

3.7 Comparative antibacterial potential of green synthesized ZnO nanoparticles

The antibacterial activity observed for the ZnO NPs derived from the extract of *Croton macrostachyus* is in good agreement with the observed trend for ZnO NPs derived from other green synthesis methods (Table 7). The range of MIC values (3.125–6.25 µg mL^{-1}) for the ZnO NPs in this study is comparable to the highest performing ZnO NPs in the most recent literature, such

Table 7 Comparative analysis of *Croton macrostachyus* Hochst. ex Delile-mediated synthesized ZnO nanoparticles

Study	Plant extract/system	Particle size (nm)	Surface chemistry/defects	Antibacterial performance (MIC or ZOI)	Mechanistic notes
Current work	*Croton macrostachyus* leaf/seed extracts	40–42 nm	Oxygen vacancies, chemisorbed oxygen, Ca/Mg traces	MIC: 3.125–6.25 µg mL^{-1}	Defect-rich surface increases the formation of ROS and Zn^{2+} dissolution
Artemisia-ZnO NPs[65]	*Artemisia absinthium* extract	36.6 nm	Polyphenol/flavonoid capping	Lower MICs than pure ZnO (qualitatively reported)	Synergistic phytochemical–ZnO ROS enhancement
Acorn fruit–ZnO NPs[66]	*Acorn* fruit extract	Very small (SEM)	Strong Zn–O FTIR signatures	*S. aureus*: 17–26 mm; *E. coli*: 15–24 mm (10–80 µg mL^{-1})	Small size enhances membrane interactions and ROS
Platycladus ZnO & Co-doped ZnO[67]	*Platycladus* leaf extract	26.9 nm (ZnO); 19 nm (Co–ZnO)	Lattice microstrain, defect generation	ZOI: 13.5–14.05 mm across multiple strains	Co doping provides more defect sites for the formation of ROS
Aloe vera ZnO NPs[49]	*Aloe vera* leaf extract	25 nm	Pure crystalline state	ZOI: 22 ± 0.4 mm; *Kosakonia Cowanii*	Oxygen vacancy-mediated ROS mechanisms

as *Artemisia* mediated ZnO NPs that have also demonstrated enhanced antibacterial activity due to the synergistic effect of the phytoconstituents used as capping agents. The ZnO NPs derived from the extract of *Acorn* have also demonstrated excellent antibacterial activity with zone inhibitions ranging from 15–26 mm for *S. aureus* and *E. coli* at similar concentration ranges to the ZnO NPs in this study. Although the crystallite sizes for the ZnO NPs in this study are slightly larger at 40–42 nm compared to the approximately 36.6 nm for the ZnO NPs derived from the extract of *Artemisia*, they are significantly larger than the approximately 19–27 nm for the defect.[65–67]

The XPS results verify that our ZnO NPs contain oxygen vacancies, chemisorbed oxygen species, and trace amounts of Mg/Ca ions, all of which are known to play a crucial role in enhancing the production of ROS and interaction of ZnO with bacteria. This is similar to that of *Aloe*-derived ZnO NPs, in which defect-related emission is associated with potent antibacterial activities. Therefore, in spite of a slightly larger particle size, the combined effect of surface defects, phytochemical capping, and nanometric dimensions is responsible for the potent bactericidal activities of our ZnO NPs. Overall, from the above comparisons, it is clear that the antimicrobial activities of our ZnO-based materials are in compliance with or even better than those of ZnO nanoparticles synthesized using green chemistry methods in the recent literature.

4 Conclusion

This paper has been able to effectively demonstrate an eco-friendly method for the biogenesis of zinc oxide nanoparticles (ZnO NPs) by exploiting aqueous leaf and seed extracts of *Croton macrostachyus* Hochst. ex Delile as reducing and stabilizing reagents. The biogeneic ZnO NPs were found to have a hexagonal wurtzite crystalline nature, nanometric size of 40.28 nm and 41.16 nm, and respective optical band gap values of 3.17 eV and 3.19 eV. This has been validated by various spectroscopic and imaging techniques like UV-Vis spectroscopy, FTIR, XRD, and SEM analysis. ZnO NPs and crude extracts have been observed to possess appreciable antibacterial properties against Gram positive and Gram negative bacteria. In view of these exciting findings, future studies must therefore concentrate on broadening the range of green synthesis by testing other Croton species for nanoparticle synthesis. *In vivo* experiments are highly recommended to authenticate biological activities as well as toxicology parameters. In addition, taking into consideration the remarkable antibacterial properties of ZnO NPs relative to raw extracts, their use in life sciences and antimicrobial applications must be thoroughly pursued. Great emphasis must thus be put on scalable green synthesis using plant extracts and other ecologically friendly biological materials in an attempt to shun traditional chemical routes.

Author contributions

Conceptualization, T. H. H. and G. M. A.; methodology, T. H. H. and G. M. A.; validation, T. H. H. and G. M. A.; formal analysis, T. H. H. and G. M. A.; investigation, S. H. A.; data curation, T. H. H. and G. M. A.; writing—original draft preparation, T. H. H. and S. H. A.; writing—review and editing, T. H. H., S. H. A., and G. M. A.; visualization, T. H. H., S. H. A., and G. M. A.; supervision, T. H. H. and G. M. A. All authors have read and agreed to the published version of the manuscript.

Conflicts of interest

The authors have declared no conflicts of interest.

Data availability

The data supporting this article have been included as part of the supplementary information (SI). Supplementary information: Tables S1–S3. See DOI: https://doi.org/10.1039/d6ra00724d.

Acknowledgements

We would like to thank the Chemistry and Biology Department of Wolaita Sodo University, who provided the lab facilities that were essential in doing these studies. In addition, we thank F. B. S. from the department of medical Microbiology of Wolaita Sodo University, who made it easy to obtain the pathogenic samples required in carrying out our studies. Finally, we thank Y. A. G. for his contributions in discussing our XPS and EDS results on our samples.

References

1 S. Anjum, S. Ishaque, H. Fatima, W. Farooq, C. Hano, B. H. Abbasi and I. Anjum, *Pharmaceuticals*, 2021, **14**, 707.
2 M. A. M. Ferreira and J. A. Filipe, in *Computational Approaches in Biomedical Nano-Engineering*, 2018, pp. 23–41, DOI: 10.1002/9783527344758.ch2.
3 H. Arif, S. Qayyum, W. Akhtar, I. Fatima, W. K. Kayani, K. U. Rahman, W. A. Al-Onazi, A. M. Al-Mohaimeed, N. K. Bangash, N. Ashraf, S. A. Razak, A. Kamal and S. Ali, *Micromachines*, 2023, **14**, 1285.
4 A. B. Shcherbakov, V. V. Reukov, A. V. Yakimansky, E. L. Krasnopeeva, O. S. Ivanova, A. L. Popov and V. K. Ivanov, *Polymers*, 2021, **13**, 924.
5 A. M. Al-Mohaimeed, W. A. Al-Onazi and M. F. El-Tohamy, *Molecules*, 2022, **27**, 579.
6 A. Rabajczyk, M. Zielecka, R. Porowski and P. K. Hopke, *Environ. Sci.: Nano*, 2020, **7**, 3233–3254.
7 V. V. Mody, R. Siwale, A. Singh and H. R. Mody, *J. Pharm. BioAllied Sci.*, 2010, **2**, 282–289.
8 M. Huston, M. DeBella, M. DiBella and A. Gupta, *Nanomaterials*, 2021, **11**, 2130.
9 M. Nasrollahzadeh, M. Sajjadi, J. Dadashi and H. Ghafuri, *Adv. Colloid Interface Sci.*, 2020, **276**, 102103.
10 F. Khan, M. Shariq, M. Asif, M. A. Siddiqui, P. Malan and F. Ahmad, *Nanomaterials*, 2022, **12**, 673.
11 S. Kar, H. Sanderson, K. Roy, E. Benfenati and J. Leszczynski, *Chem. Rev.*, 2022, **122**, 3637–3710.

12 O. A. L. dos Santos, B. Pizzorno Backx, R. A. Abumousa and M. Bououdina, *Nanomaterials*, 2022, **12**, 4319.

13 A. Chatterjee, N. Kwatra and J. Abraham, in *Phytonanotechnology*, ed. N. Thajuddin and S. Mathew, Elsevier, 2020, pp. 143–157, DOI: 10.1016/B978-0-12-822348-2.00008-5.

14 G. Sharmila, M. Thirumarimurugan and C. Muthukumaran, *Microchem. J.*, 2019, **145**, 578–587.

15 N. N. Son, V. M. Thanh and N. T. Huong, *ChemistrySelect*, 2023, **8**, e202303214.

16 S. Vijayakumar, B. Vaseeharan, B. Malaikozhundan and M. Shobiya, *Biomed. Pharmacother.*, 2016, **84**, 1213–1222.

17 K. Ali, S. Dwivedi, A. Azam, Q. Saquib, M. S. Al-Said, A. A. Alkhedhairy and J. Musarrat, *J. Colloid Interface Sci.*, 2016, **472**, 145–156.

18 J. K. Obey, M. M. Ngeiywa, P. Kiprono, S. Omar, A. von Wright, J. Kauhanen and C. Tikkanen-Kaukanen, *J. Pathog.*, 2018, **2018**, 2393854.

19 A. Maroyi, *J. Evidence-Based Complementary Altern. Med.*, 2017, **2017**, 1694671.

20 A. R. Prasad, L. Williams, J. Garvasis, K. O. Shamsheera, S. M. Basheer, M. Kuruvilla and A. Joseph, *J. Mol. Liq.*, 2021, **331**, 115805.

21 A. Castillo, M. Celeiro, M. Lores, K. Grgić, M. Banožić, I. Jerković and S. Jokić, *Mar. Drugs*, 2023, **21**, 97.

22 S. Lamponi, *Plants*, 2021, **10**, 1225.

23 A. R. Deshmukh and B. S. Kim, in *Phytonanotechnology*, ed. N. Thajuddin and S. Mathew, Elsevier, 2020, pp. 97–121, DOI: 10.1016/B978-0-12-822348-2.00006-1.

24 J. Xie, H. Li, T. Zhang, B. Song, X. Wang and Z. Gu, *Nanomaterials*, 2023, **13**, 1500.

25 T. Biswas, S. S. S. Kubra and S. Awasthi, *BioNanoScience*, 2024, **14**, 581–593.

26 S. M. Mengesha, G. M. Abebe and T. H. Habtemariam, *Sci. Rep.*, 2024, **14**, 23870.

27 S. Rai, E. Acharya-Siwakoti, A. Kafle, H. P. Devkota and A. Bhattarai, *Science*, 2021, **3**, 44.

28 S. Dubale, D. Kebebe, A. Zeynudin, N. Abdissa and S. Suleman, *J. Exp. Pharmacol.*, 2023, **15**, 51–62.

29 B. Ndezo Bisso, R. Njikang Epie Nkwelle, R. Tchuenguem Tchuenteu and J. P. Dzoyem, *Adv. Pharmacol. Pharm. Sci.*, 2022, **2022**, 1998808.

30 N. Bakir Çilesizoğlu, E. Yalçin, K. Çavuşoğlu and S. Sipahi Kuloğlu, *Sci. Rep.*, 2022, **12**, 21421.

31 M. Balouiri, M. Sadiki and S. K. Ibnsouda, *J. Pharm. Anal.*, 2016, **6**, 71–79.

32 R. Mogana, A. Adhikari, M. N. Tzar, R. Ramliza and C. Wiart, *BMC Complementary Med. Ther.*, 2020, **20**, 55.

33 S. Salloum, J. Rüther, Z. Celik and C. Janiak, *Nanoscale*, 2025, **17**, 23373–23386.

34 P. K. Dikshit, J. Kumar, A. K. Das, S. Sadhu, S. Sharma, S. Singh, P. K. Gupta and B. S. Kim, *Catalysts*, 2021, **11**, 902.

35 A. Pach, A. Szot, K. Fitzner and M. Luty-Błocho, *Micromachines*, 2024, **15**, 1119.

36 A. Singh and U. Mina, *Physiol. Mol. Biol. Plants*, 2025, **31**, 675–692.

37 H. Tang, X. Wu, H. Xian, J. Zhu, J. Wei, H. Liu and H. He, *Minerals*, 2020, **10**, 294.

38 C. Chen, H. Zhong, X. Wang, M. Ning, X. Wang, Y. Ge, H. Wang, R. Tang and M. Hou, *Minerals*, 2023, **13**, 1479.

39 V. Kumar, S. Kaushal and Y. Singh, *New J. Chem.*, 2025, **49**, 16145–16159.

40 P. Ravi, M. C. Reddy, T. Chandrasekhar, S. V. Chinni, H. Adam, S. C. B. Gopinath and V. R. Lebaka, *J. Cluster Sci.*, 2024, **36**, 8.

41 G. P. Lopinski, O. Kodra, F. Kunc, D. C. Kennedy, M. Couillard and L. J. Johnston, *Nanoscale Adv.*, 2025, **7**, 1671–1685.

42 T. V. Nitha and S. Britto, *J. Iran. Chem. Soc.*, 2025, **22**, 915–929.

43 W.-B. Zhao, M.-R. Du, K.-K. Liu, R. Zhou, R.-N. Ma, Z. Jiao, Q. Zhao and C.-X. Shan, *ACS Appl. Mater. Interfaces*, 2020, **12**, 13305–13315.

44 A. R. Abhijith, T. T. Mashangva, H. Sharma, A. Srivastava and R. Thomas, *J. Mater. Sci.: Mater. Electron.*, 2025, **36**, 1275.

45 S. Mrabet, N. Ihzaz, M. N. Bessadok, C. Vázquez-Vázquez, M. Alshammari and L. El Mir, *J. Inorg. Organomet. Polym. Mater.*, 2024, **34**, 2064–2073.

46 A. L. C. Silva, L. M. B. Vargas, M. L. Peres, M. D. Teodoro and M. P. F. de Godoy, *Coatings*, 2024, **14**, 510.

47 L. H. Grey, H.-Y. Nie and M. C. Biesinger, *Appl. Surf. Sci.*, 2024, **653**, 159319.

48 V. N. Jafarova and G. S. Orudzhev, *Solid State Commun.*, 2021, **325**, 114166.

49 C. Wu, T. Zhang, B. Ji, Y. Chou and X. Du, *Cellulose*, 2024, **31**, 4849–4864.

50 I. Ngom, B. D. Ngom, J. Sackey and S. Khamlich, *Mater. Today: Proc.*, 2021, **36**, 526–533.

51 N. Rani, S. Yadav, A. Mushtaq, S. Rani, M. Saini, S. Rawat, K. Gupta, K. Saini and D. Maity, *Chem. Pap.*, 2024, **78**, 3687–3704.

52 S. B. Endeshaw, L. T. Tufa, M. Goddati, J. Lee, V. C. Silalahi, D. Lee, H. C. A. Murthy and F. K. Sabir, *ACS Omega*, 2024, **9**, 559–572.

53 T. Jabessa Masho, P. Thillai Arasu, R. Feyisa Bogale, E. Amare Zerrefa and S. Ramamurthy, *Results Chem.*, 2024, **7**, 101369.

54 D. C. Bouttier-Figueroa, M. Cortez-Valadez, M. Flores-Acosta and R. E. Robles-Zepeda, *BioNanoScience*, 2024, **14**, 3385–3400.

55 O. A. Zelekew, H. H. Haitosa, X. Chen and Y.-N. Wu, *Adv. Colloid Interface Sci.*, 2023, **317**, 102931.

56 I. El-Habib, H. Maatouk, A. Lemarchand, S. Dine, A. Roynette, C. Mielcarek, M. Traoré and R. Azouani, *J. Funct. Biomater.*, 2024, **15**, 195.

57 R. Goyal, P. Roy and P. Jeevanandam, *Appl. Phys. A*, 2023, **129**, 244.

58 J. Nan, Y. Chu, R. Guo and P. Chen, *Front. Mater.*, 2024, **11**, 1449614.

59 C. R. Mendes, G. Dilarri, C. F. Forsan, V. d. M. R. Sapata, P. R. M. Lopes, P. B. de Moraes, R. N. Montagnolli, H. Ferreira and E. D. Bidoia, *Sci. Rep.*, 2022, **12**, 2658.

60 A. R. Mendes, C. M. Granadeiro, A. Leite, E. Pereira, P. Teixeira and F. Poças, *Nanomaterials*, 2024, **14**, 638.

61 S. Tiwari, O. Nizet and N. Dillon, *Front. Microbiol.*, 2023, **14**, 1079033.

62 N. Pangprasit, A. Kongkaew, D. Saipinta, S. Pikulkaew, M. Intanon, W. Suriyasathaporn and W. Chaisri, *Pharmaceutics*, 2025, **17**, 209.

63 F. Alhosani, D. Islayem, S. Almansoori, A. Zaka, L. Nayfeh, A. Rezk, A. F. Yousef, A. M. Pappa and A. Nayfeh, *Sci. Rep.*, 2025, **15**, 17321.

64 S. K, S. Nechikkadan, M. Theresa and R. E. Krishnankutty, *Folia Microbiol.*, 2024, **69**, 1175–1183.

65 N. Akhras, A. Çelekli and H. Bozkurt, *Foods*, 2025, **14**, 2449.

66 M. Umar, M. Ahmad, M. Sadeeq, H. Ali, A. Khan, A. A. Chaudry, M. A. M. Ali and M. U. Naeem, *Sci. Rep.*, 2026, **16**, 7072.

67 M. C. Ogwuegbu, O. C. Olatunde, T. M. Pfukwa, D. M. N. Mthiyane, O. A. Fawole and D. C. Onwudiwe, *Discover Mater.*, 2025, **5**, 55.